Co-published by
Institute of Fluid-Flow Machinery
Polish Academy of Sciences
Committee on Thermodynamics and Combustion
Polish Academy of Sciences

http://www.imp.gda.pl/archives-of-thermodynamics/

Numerical study of radiating Casson fluid past a permeable stretching sheet in a Darcy-Forchheimer porous medium

Shish Ram Dhwal[a*], Rajendra Singh Yadav[a], Oluwole Daniel Makinde[b]

[a]Department of Mathematics, University of Rajasthan, Rajasthan, Jaipur 302004, India
[b]Faculty of Military Science Stellenbosch University, Stellenbosch, Western Cape, South Africa
*Corresponding author email: shishramdhwal75@gmail.com

Received: 21.11.2024; revised: 16.02.2025; accepted: 20.03.2025

Abstract

This research investigates the mixed convection of an incompressible, non-Newtonian radiating Casson fluid in a Darcy-Forchheimer porous medium over a slippery, permeable, stretching surface. The study further examines the influences of thermal buoyancy and viscous dissipation. Through appropriate similarity transformations, the governing nonlinear partial differential equations are transformed into nonlinear ordinary differential equations. These nonlinear ordinary differential equations are solved using MATLAB with the fourth-order Runge-Kutta method combined with the shooting technique. This work aims to assess the influence of Casson parameter, porosity parameter, radiation parameter, suction parameter, Eckert number, mixed convection parameter, local inertia coefficient, Prandtl number and slip parameter on the velocity and temperature. The findings show that increasing Casson parameter results in decreased velocity and temperature, while an increase in the radiation parameter leads to a rise in temperature. Velocity decreases with an increase in slip parameter for velocity, but as the similarity variable exceeds 2.4, it experiences a slight increase due to the stretching effect of the sheet. Conversely, temperature is directly proportional to slip parameter for velocity.

Keywords: Darcy-Forchheimer porous medium; Permeable stretching sheet; Radiating Casson fluid; Thermal buoyancy; Viscous dissipation

Vol. 46(2025), No. 2, 199–208; doi: 10.24425/ather.2025.154918

Cite this manuscript as: Dhwal, S.R., Yadav, R.S., & Makinde, O.D. (2025). Numerical study of radiating Casson fluid past a permeable stretching sheet in a Darcy-Forchheimer porous medium. *Archives of Thermodynamics*, 46(2), 199–208.

1. Introduction

The exponential stretching surface in boundary layer flow has significant applications in manufacturing engineering, such as the production of copper wires and determining the quality of various industrial products. A substantial portion of contemporary research focuses on the study of boundary layer flow over stretching sheets. For instance, Gupta and Gupta [1] analysed the transfer of momentum, mass, and heat within the boundary region of a stretching sheet. Magyari and Keller [2], along with Elbashbeshy [3], investigated heat transfer over an exponentially stretched sheet, considering the effects of suction and blowing. Pramanik [4] examined heat transfer in the boundary layer of an exponentially stretching surface. Jain et al. [5] studied boundary layer flow over a suction surface with slip and mixed convection conditions. Similarly, researchers like Partha et al. [6], Khan [7], and Sajid and Hayat [8] explored exponentially stretching sheets under various fluid dynamics scenarios.

Nomenclature

C_p – specific heat coefficient, J/(kg K)
C_f – skin friction coefficient
e_{ij} – (ij)th component of the deformation rate
Ec – Eckert number
f – dimensionless stream function
F – drag coefficient
Fr – local inertia coefficient
g – gravitational acceleration, m/s^2
Gr – Grashof number
h – heat transfer coefficient, W/ (m^2 K)
K – porous medium permeability, m^2
K_1 – porosity parameter
k^* – mean absorption coefficient, 1/m
L – characteristic length, m
N – radiation parameter
Nu – Nusselt number
Pr – Prandtl number
q – heat flux, W/m^2
R – slip length coefficient, m
Re – Reynolds number
S – suction/blowing parameter
T – temperature, K
u, v– velocity in x- and y-direction, m/s
U – stretching velocity, m/s
V – velocity over the sheet, m/s

Greek symbols

β – Casson parameter
β^* – thermal expansion coefficient, 1/K
θ – dimensionless temperature
ϑ – kinematic viscosity, m^2/s
κ – thermal conductivity, W/(m K)
λ – mixed convection parameter
λ_u – slip parameter for velocity
λ_t – slip parameter for temperature
μ – viscosity of fluid, Pa·s
η – similarity variable
ρ – density, kg/m^3
σ – Stefan-Boltzmann coefficient, 5.67×10^{-8} W/(m^2 K^4)

Subscripts and Superscripts

r – radiation,
t – temperature
u – velocity
W – sheet surface
0 – initial
∞ – fluid surface
$(\cdot)'$ – differentiation with respect to η

Abbreviations and Acronyms

PDE – partial differential equation
ODE – ordinary differential equation

The study of radiating Casson fluid flow holds diverse engineering and industrial applications, particularly in fluid dynamics and complex fluid behaviours. It is relevant in processes such as polymer processing, food manufacturing, paint production, and oil drilling. Additionally, the non-Newtonian behaviour of blood can be described using the Casson fluid model, which is critical for designing medical devices like artificial heart valves and understanding blood circulation mechanics. Radiating Casson fluid also plays a role in studying blood flow under different physiological conditions. For example, during cardiac surgeries, external heating or cooling is used to regulate blood flow and prevent complications. Bejawada et al. [9] investigated the effects of radiating Casson fluid flow in a porous medium with an inclined non-linear sheet, while Rassol et al. [10] explored Casson nanofluid flow in a porous medium over a non-linear stretching sheet. Bilal et al. [11] provided an analytical study on Casson fluid flow over an isothermal sloping Riga sheet with thermal radiation. Other notable works include Raju et al. [12], who analysed heat and mass transfer characteristics of Casson fluid on a rotating wedge under thermal radiation, and Mehmood et al. [13], who studied the behaviour of non-aligned Casson fluid on a stretching surface in the presence of radiation. Research by Sinha et al. [14] focused on mixed convection in fluid flow with dissipation and radiation effects, while Loganathan and Deepa [15] examined electromagnetic and radiative Casson fluid flow near a permeable vertical plate. Additional studies by Kumar and Sugunamma [16] and Samrat et al. [17] investigated magnetohydrodynamic (MHD) radiative Casson fluid over various geometries.

Viscous dissipation, an essential concept in fluid mechanics, refers to the conversion of mechanical energy into thermal energy due to internal friction within a fluid. This phenomenon is influenced by fluid viscosity and shear forces and plays a vital role in applications like heat exchangers, cooling systems, and electronics cooling. Gebhart [18] was the first to discuss the viscous dissipation term in natural convection, while Hadhrami et al. [19] studied its effects on porous media and permeable surfaces. Hayat et al. [20] explored the impact of viscous dissipation in Casson fluid flow combined with nanofluid and thermal conductivity. Praveen et al. [21] examined Joule heating and heat generation effects on a permeable stretching cylinder. Researchers such as Koo and Kleinstreuer [22] and Winter [23] have also investigated the role of viscous dissipation in energy equations.

The Darcy-Forchheimer porous medium is used to model fluid flow in filtration processes, water treatment systems, and oil and gas filtration. It is also applied in geotechnical engineering to estimate groundwater flow rates and pressure distributions and has biomedical applications in tissue engineering, drug delivery, and blood flow through tissues. For example, Khan [24] analysed velocity slip, viscous dissipation, heat sources/sinks, and Ohmic heating in a Darcy-Forchheimer porous medium. Mukhopadhyay et al. [25] studied boundary layer convective flow over a porous plate in such a medium. Ganesh et al. [26] investigated heat transfer in non-Newtonian Reiner-Philippoff fluid flow within a Darcy-Forchheimer medium, while Prasad [27] examined thermal diffusion in MHD mixed convection over an accelerating vertically wavy plate in a porous medium. Shoaib et al. [28] analysed the effects of a Forchheimer porous medium on Casson fluid over a non-linear surface, and Bansal

and Yadav [29] explored slip velocity effects in Newtonian fluid flow over a stretching surface with a porous medium.

This research expands on the work of Pramanik [4] by incorporating the effects of slippery, permeable Darcy-Forchheimer porous medium and mixed convection. The effects of slip conditions, viscous dissipation, and thermal buoyancy are also investigated. The governing nonlinear partial differential equations are transformed into nonlinear ordinary differential equations using similarity transformations. These equations are solved numerically using the fourth-order Runge-Kutta method.

2. Mathematical model

This study focuses on the incompressible, non-Newtonian radiative Casson fluid over a slippery, permeable, stretching flat surface. The flow occurs within a Darcy-Forchheimer porous medium, with the flat plate aligned parallel to the x-axis (Fig. 1). Fluid stream is restricted to $y > 0$. Further assumptions include that two identical but adverse stresses are used along with the flow direction to stretch the sheet while maintaining the origin static. The phenomena impacting the fluid flow include radiative heat transfer, drag effects, buoyancy forces, and viscous dissipation.

The following equation is the rheological expression for an incompressible, isotropic, and viscous Casson fluid:

$$\tau_{ij} = \begin{cases} 2\left(\mu_B + \frac{p_y}{\sqrt{2\pi}}\right) e_{ij}, & \pi > \pi_c \\ 2\left(\mu_B + \frac{p_y}{\sqrt{2\pi_\epsilon}}\right) e_{ij}, & \pi < \pi_c \end{cases},$$

where $\pi = e_{ij}e_{ij}$ is the product of the component of deformation rate, e_{ij} is the (ij)th component of the deformation rate, μ_B is the plastic dynamic viscosity of a non-Newtonian fluid, p_y is the yield stress of the fluid, and π_c is the critical value of the product.

The governing continuity equation, derived from the principle of mass conservation for an incompressible fluid in two dimensions, is expressed as

$$\frac{\partial u}{\partial x} + \frac{\partial v}{\partial y} = 0, \tag{1}$$

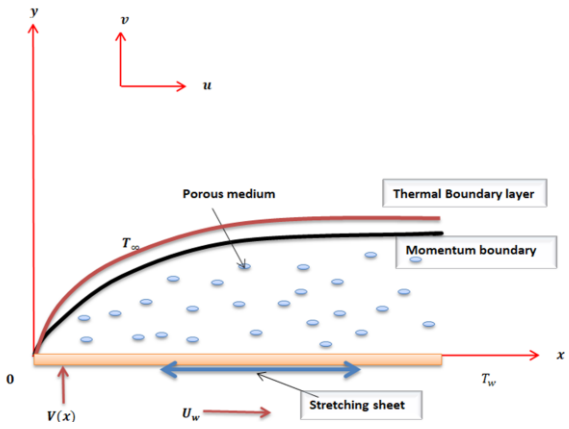

Fig. 1. Diagram of the flow case under consideration.

where u is the velocity in the x-direction, and v is the velocity in the y-direction.

The momentum equation, also called the Navier-Stokes equation, is derived from Newton's second law of motion for an incompressible non-Newtonian fluid, incorporating additional effects such as permeability, buoyancy and a stretching sheet, and is expressed as

$$u\frac{\partial u}{\partial x} + v\frac{\partial u}{\partial y} = \vartheta\left(1+\frac{1}{\beta}\right)\frac{\partial^2 u}{\partial y^2} - \vartheta\left(1+\frac{1}{\beta}\right)\frac{u}{K} + \\ -\frac{Fu^2}{\rho\sqrt{K}} + g\beta^*(T - T_\infty), \tag{2}$$

where ρ is the density, β^* is the thermal expansion, ϑ is the kinematic viscosity, F is the drag coefficient, g is the gravitational acceleration, K is the permeability of the porous medium, T is the temperature, and $\beta = \mu_B\frac{\sqrt{2\pi_c}}{p_y}$ is the Casson parameter.

The energy equation, derived from the first law of thermodynamics (the conservation of energy), for an incompressible non-Newtonian fluid with effects, such as porous medium, viscous dissipation, Forchheimer drag, and radiative heat transfer, is expressed as

$$u\frac{\partial T}{\partial x} + v\frac{\partial T}{\partial y} = \frac{\kappa}{\rho C_p}\frac{\partial^2 T}{\partial y^2} + \frac{\mu}{\rho C_p}\left(1+\frac{1}{\beta}\right)\left(\frac{\partial u}{\partial y}\right)^2 + \\ + \left(1+\frac{1}{\beta}\right)\frac{\mu u^2}{K\rho C_p} + \frac{Fu^3}{\rho C_p\sqrt{K}} - \frac{1}{\rho C_p}\frac{\partial q_r}{\partial y}. \tag{3}$$

where C_p is the specific heat, q_r is the radiative heat flux, κ is the thermal conductivity, and μ is the viscosity. We are able to write an expression of the Rosseland estimation as

$$q_r = -\frac{4\sigma}{3k^*}\frac{\partial T^4}{\partial y}, \tag{4}$$

where σ is the Stefan-Boltzmann constant and k^* is the mean absorption coefficient. Then, expanding T^4 along with T_∞ with the help of Taylor series, taking zero of higher-order terms in fluid flow yields:

$$T^4 \equiv 4T_\infty^3 T - 3T_\infty^4. \tag{5}$$

Using Eqs. (4) and (5), Eq. (3) is converted into

$$u\frac{\partial T}{\partial x} + v\frac{\partial T}{\partial y} = \left(\frac{\kappa}{\rho C_p} + \frac{16\sigma T_\infty^3}{3\rho C_p k^*}\right)\frac{\partial^2 T}{\partial y^2} + \frac{\mu}{\rho C_p}\left(1+\frac{1}{\beta}\right)\left(\frac{\partial u}{\partial y}\right)^2 + \\ + \left(1+\frac{1}{\beta}\right)\frac{\mu u^2}{K\rho C_p} + \frac{Fu^3}{\rho C_p\sqrt{K}}. \tag{6}$$

The boundary conditions adopted in this study are:

$$u = U_w + \frac{\mu}{R}\left(1+\frac{1}{\beta}\right)\frac{\partial u}{\partial y}, \\ v = -V(x), \qquad \text{at } y = 0, \\ -\kappa\frac{\partial T}{\partial y} = h(T_w - T), \tag{7}$$

$$u \to 0, \quad T \to T_\infty \quad \text{as } y \to \infty \tag{8}$$

Here, $U_w = U_0 e^{\frac{x}{L}}$ is the stretch velocity, where L is the is the characteristic length and U_0 is the reference velocity, R is the

slip length coefficient, $T_w = T_0 e^{\frac{x}{2L}}$ is the temperature over the surface, T_0 is the reference temperature, $V(x) = V_0 e^{\frac{x}{2L}}$ is a velocity over the sheet, where V_0 is considered as constant, while $V(x) > 0$ is the velocity for suction and $V(x) < 0$ is the velocity for blowing.

3. Numerical solution

Dimensionless variables are defined as:

$$\eta = \sqrt{\frac{U_0}{2\vartheta L}}\, e^{\frac{x}{2L}} y, \quad v = -\sqrt{\frac{\vartheta U_0}{2L}} e^{\frac{x}{2L}} \left[f(\eta) + \eta f'^{(\eta)}\right], \quad u = U_0 e^{\frac{x}{L}} f'(\eta), \quad T = T_\infty + T_0 e^{\frac{x}{2L}} \theta(\eta), \tag{9}$$

where f is the dimensionless stream function and θ is the dimensionless temperature, and the prime mark denotes differentiation with respect to η.

Using Eqs. (9), Eqs. (2) and (6) transform to dimensionless forms, respectively:

$$\left(1+\frac{1}{\beta}\right) f''' + f f'' - \left(1+\frac{1}{\beta}\right) K_1 f' - (\mathrm{Fr}+2) f'^2 + 2\lambda\theta = 0, \tag{10}$$

$$\left(1+\frac{4}{3}N\right)\theta'' - \mathrm{Pr}(\theta f' - f\theta') + \left(1+\frac{1}{\beta}\right)\mathrm{EcPr}\left(f''^2 + K_1 f'^2\right) + \mathrm{FrEcPr} f'^3 = 0, \tag{11}$$

where higher order derivatives with respect to η are represented by adding more primes (the second and third derivatives).

Applying similarity transformation from Eq. (9), Eqs. (7) and (8) can be converted as follows:

$$\begin{cases} f'(0) = 1 + \left(1+\frac{1}{\beta}\right)\lambda_u + f'', \\ f'(0) = S, \\ \theta(0) = 1 + \lambda_t \theta'(0), \end{cases} \quad \text{at } \eta = 0, \tag{12}$$

$$f'(\infty) \to 0, \quad \theta(\infty) \to 0, \quad \text{as } \eta \to \infty. \tag{13}$$

Here, $S = \frac{V_0}{\sqrt{\frac{\vartheta U_0}{2L}}} > 0$ is the suction or $S < 0$ is the blowing parameter, $\lambda_u = \frac{\mu}{R}\sqrt{\frac{U_0}{2\vartheta L}} e^{\frac{x}{2L}}$ is the velocity slip parameter, $\lambda_t = \frac{\kappa}{h}\sqrt{\frac{U_0}{2\vartheta L}} e^{\frac{x}{2L}}$ is the slip parameter of temperature distribution, $\mathrm{Gr} = \frac{g\beta^*(T_w - T_\infty)L^3}{\vartheta^2}$ is the Grashof number, $\mathrm{Pr} = \frac{\mu C_p}{\kappa}$ is the Prandtl number, $\mathrm{Ec} = \frac{{U_w}^2}{C_p(T_w - T_\infty)}$ is the Eckert number, $\mathrm{Fr} = \frac{2FL}{\rho\sqrt{\kappa}}$ is the local inertia coefficient, $\lambda = \frac{\mathrm{Gr}}{\mathrm{Re}^2}$ is the mixed convection parameter, $\mathrm{Re}^2 = \frac{{U_w}^2 L^2}{\vartheta}$ is the local Reynolds number, $K_1 = \frac{2\vartheta L}{U_w K}$ – the porosity parameter, $N = \frac{4\sigma T_\infty^3}{\kappa k^*}$ – the radiation parameter.

The skin friction coefficient C_f and Nusselt number Nu, which are the factors of physical interest, are calculated as

$$C_f = \frac{\tau_w}{\frac{1}{2}\rho U_w^2}, \quad \mathrm{Nu} = \frac{L q_w}{\kappa(T_w - T_\infty)},$$

where τ_w is the shear stress at the surface and q_w is the heat flux at the surface:

$$\tau_w = \mu\left(\frac{\partial u}{\partial y}\right)_{y=0}, \quad q_w = -\kappa\left(\frac{\partial T}{\partial y}\right)_{y=0}.$$

By using Eq. (8), the above are converted as follows:

$$C_f \frac{\sqrt{\mathrm{Re}}}{\sqrt{2}} = f''(0), \quad \mathrm{Nu}\frac{\sqrt{2}}{\sqrt{\mathrm{Re}}} = -\theta'(0).$$

3.1. Numerical methodology

Using Eqs. (12) and (13), the solution of governing Eqs. (10) and (11) has been computed numerically by means of the fourth-order Runge-Kutta (RK4) method. The momentum and energy equations are converted from higher order to first order differential equations using the following substitution:

$$f = f_1, \quad f' = f_2, \quad f'' = f_3,$$

$$f'_3 = \frac{1}{\left(1+\frac{1}{\beta}\right)}\left[\left(1+\frac{1}{\beta}\right)K_1 f_2 + (2+\mathrm{Fr}) f_2^2 - f_1 f_3 - 2\lambda f_4\right], \tag{14}$$

$$\theta = f_4, \quad \theta' = f_5,$$

$$f'_5 = \frac{1}{1+\frac{4}{3}N}\left[\mathrm{Pr}(f_4 f_2 - f_1 f_5) - \left(1+\frac{1}{\beta}\right)\mathrm{EcPr}(f_3^2 + K_1 f_2^2) + - \mathrm{FrEcPr} f_2^3\right] \tag{15}$$

with the boundary conditions:

$$\begin{cases} f_1(0) = S, \\ f_2(0) = 1 + \left(1+\frac{1}{\beta}\right)\lambda_u f_3(0), \\ f_2(0) = 1 + \left(1+\frac{1}{\beta}\right)\lambda_u f_3(0), \\ f_4(0) = 1 + \lambda_t f_5(0), \\ f_2(\infty) \to 0, \\ f_4(\infty) \to 0. \end{cases} \tag{16}$$

The values of $f_3(0)$ and $f_5(0)$ are required to integrate the initial value problems in Eqs. (14) and (15) with the boundary conditions given by Eqs. (16), but these values are not provided. It is crucial to set a finite value for η_∞ when using the shooting technique. We begin with random initial estimate values to obtain $f_3(0)$ and $f_5(0)$ for a finite value of η_∞. Repeating this process for the significant value of η_∞, a finite value of $\eta_\infty = 10$ for all physical parameters is used to integrate the boundary value problem with a difference of 0.01, applying the RK4 method. We set the better approximation of $f_3(0)$ and $f_5(0)$ for the given boundary conditions of $f_2(10) = 10$ and $f_4(10) = 0$ until the output reaches the required decimals of accuracy 10^{-5}.

3.2. Validation of the code

To verify the present code, the guessed value of $f_3(0)$ for ($\beta = \infty$) is similar to the result provided by Sahoo and Poncet [30],

Table 1. Comparison of $-\theta'(0)$ against Prandtl number for $K_1 = S = \mathrm{Fr} = \mathrm{Ec} = \lambda = \lambda_u = \lambda_t = 0$, $\beta = \infty$.

	Bidin &Nazar [31]		Pramanik [4]		Present study	
N / Pr	**0.5**	**1**	**0.5**	**1**	**0.5**	**1**
1	0.6765	0.5315	0.6765	0.5315	0.6775	0.5353
2	1.0735	0.8627	1.0734	0.8626	1.1074	0.8628
3	1.3807	1.1214	1.3807	1.1213	1.3807	1.1214

Keller and Magyari [2], and Pramanik [4] in their seminal works. The value $f_3(0) = -1.281816$ is correct up to 10^{-6}, which is a sufficient accuracy compared with $f_3(0) = -1.281811$, $f_3(0) = -1.28180$, and $f_3(0) = -1.28182$. Table 1 validates the program's coding by comparing the current outcome with the results reported by Pramanik [4] and Bidin [31].

4. Results and discussion

The combined effects of various parameters on velocity and temperature are analysed for the Casson parameter, porosity parameter, radiation parameter, suction parameter, Eckert number, mixed convection parameter, local inertia coefficient, Prandtl number, and slip parameter, while keeping the fixed values $\beta = 0.5$, $K_1 = 0.1$, $\mathrm{Pr} = 0.7$, $N = 1$, $\mathrm{Fr} = 1$, $\mathrm{Ec} = 0.2$, $\lambda = 0.5$, $\lambda_u = 0.1$, and $\lambda_t = 0.1$. Figures 2 and 3 illustrate the influence of the Casson parameter (β) on the velocity and temperature profiles. For velocity, an increase in β enhances the flow in the region approximately between $0 \le \eta \le 0.62$ ($S = 0.5$) and $0 \le \eta \le 0.86$ ($S = -0.5$). Beyond these points, an opposite trend is observed. Initially, the velocity increases due to the effect of the slippery surface. However, as β continues to rise, the fluid's yield stress increases, resulting in higher resistance forces, which ultimately reduce the fluid velocity. In terms of temperature, an increase in β leads to a reduction in the temperature profile. This behaviour is attributed to the same resistance effect caused by the increased yield stress. Additionally, when comparing the effects of blowing and suction, it is evident that suction significantly reduces both the fluid velocity and temperature.

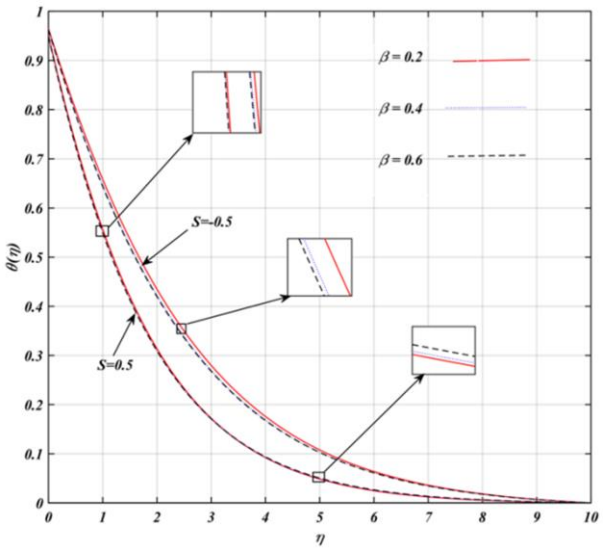

Fig. 3. Change in temperature profiles with β in the existence of S.

Figures 4 and 5 depict the effect of the suction parameter (S) on the velocity and temperature profiles. When $S > 0$ (suction), the velocity profile significantly decreases. The case $S = 0$ represents a non-permeable stretching sheet. Conversely, for $S < 0$ (blowing), the velocity exhibits an increasing trend. The temperature profile also decreases with an increase in $S > 0$, whereas it rises when $S < 0$. This behaviour can be attributed to the fact that blowing increases pressure, allowing the warmed fluid to move farther from the surface, accelerating both velocity and temperature. In contrast, suction exerts an opposite influence by

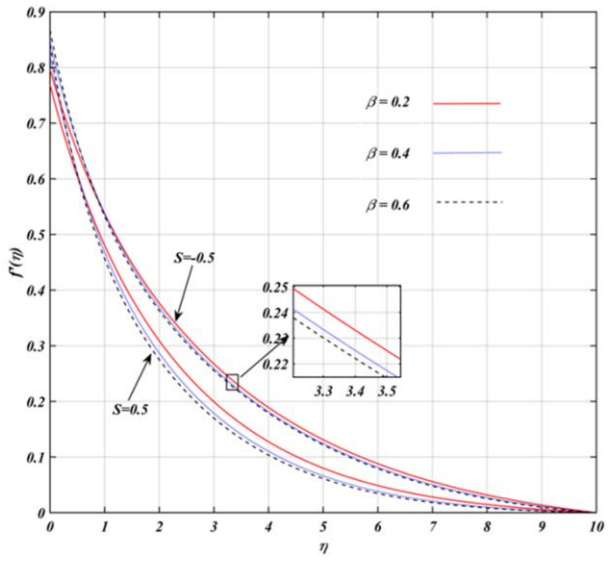

Fig. 2. Change in velocity profiles with β in the existence of S.

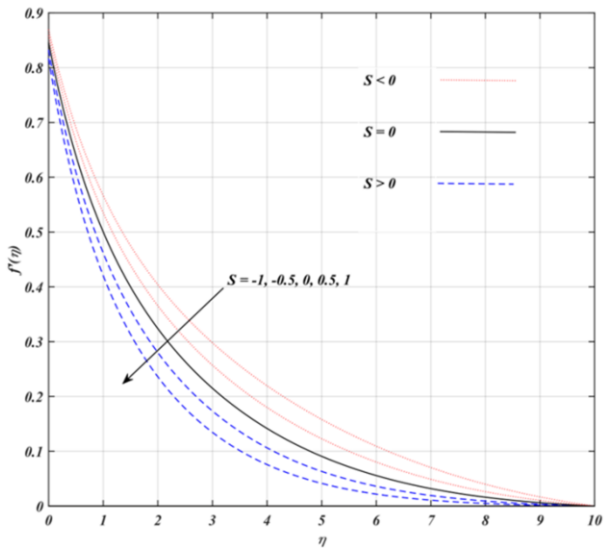

Fig. 4. Velocity profiles for varying S.

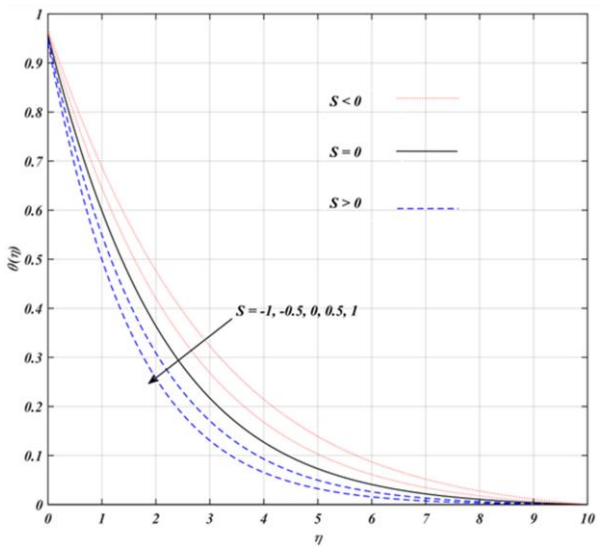

Fig.5. Temperature profiles for varying S.

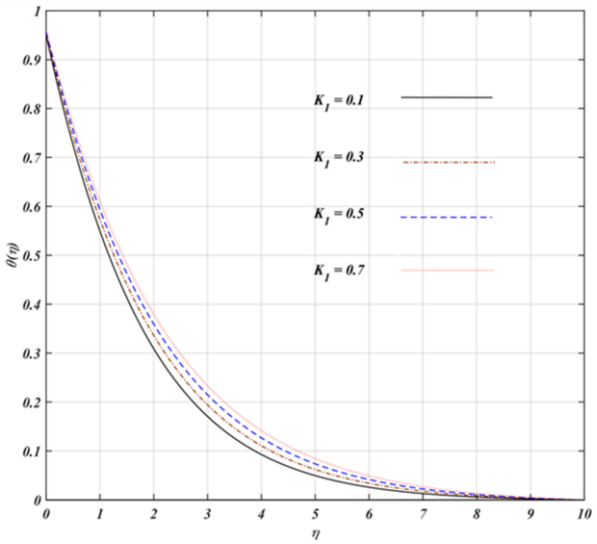

Fig. 7. Change in temperature profiles with K_1.

pulling the fluid closer to the surface, reducing both velocity and temperature.

Figures 6 and 7 present the effect of the porosity parameter (K_1) on the temperature and velocity profiles. As K_1 increases, permeability of the porous medium decreases. This reduced permeability leads to stronger resistance and, consequently, lower fluid velocity. The Forchheimer effect also contributes to increased resistance, further decreasing the velocity. This reduction in permeability and the presence of the Forchheimer effect cause an increase in resistance, which in turn leads to a higher temperature profile as K_1 increases.

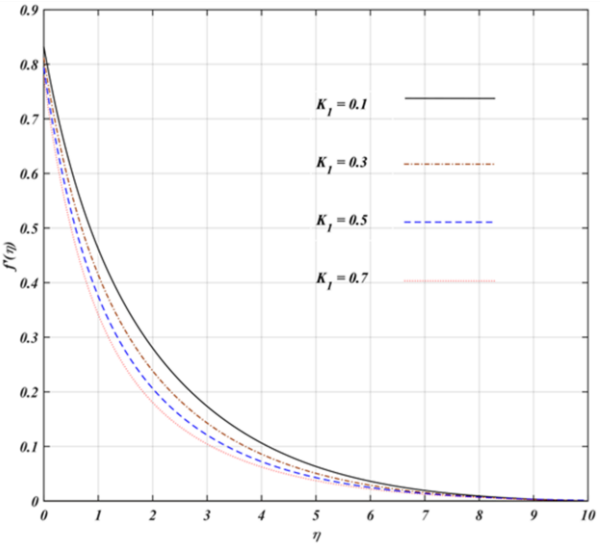

Fig.6. Change in velocity profiles with K_1.

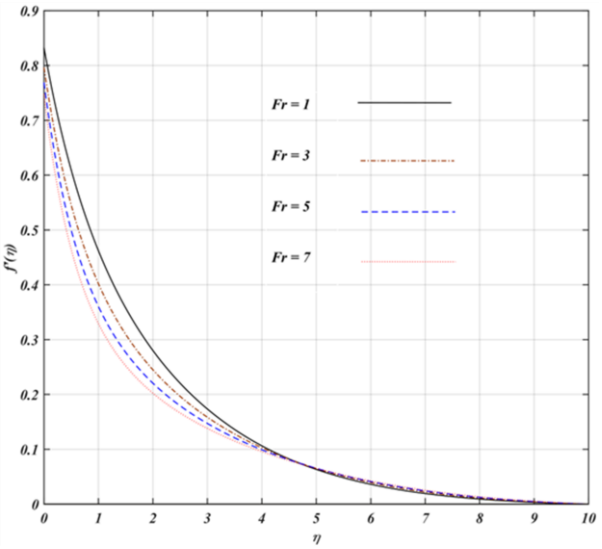

Fig. 8. Change in velocity profiles with Fr.

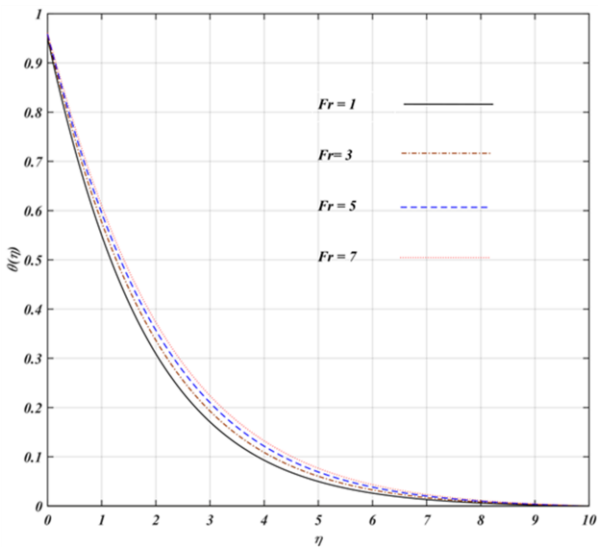

Fig. 9. Change in temperature profiles with Fr.

Figures 8 and 9 show the influence of the local inertia coefficient (Fr) on velocity and temperature. Here, the Forchheimer drag in porous medium increases internal resistance; higher Fr increases flow resistance, reducing fluid velocity in the porous medium. Forchheimer inertial drag generates heat, so a higher

Fr increases heat generation, leading to a rise in fluid temperature.

Figures 10 and 11 explore the effect of the mixed convection parameter (λ) on the velocity and temperature. The results indicate that temperature decreases and velocity increases with rising λ. This occurs because the temperature difference is directly proportional to λ; the temperature gradient at the wall increases, leading to a higher Nusselt number (more efficient heat dissipation). The thermal boundary layer thickness decreases as more heat is convected away. In the velocity case, the buoyancy force acts in the direction of the flow, which leads to an increase in velocity with an increase in λ.

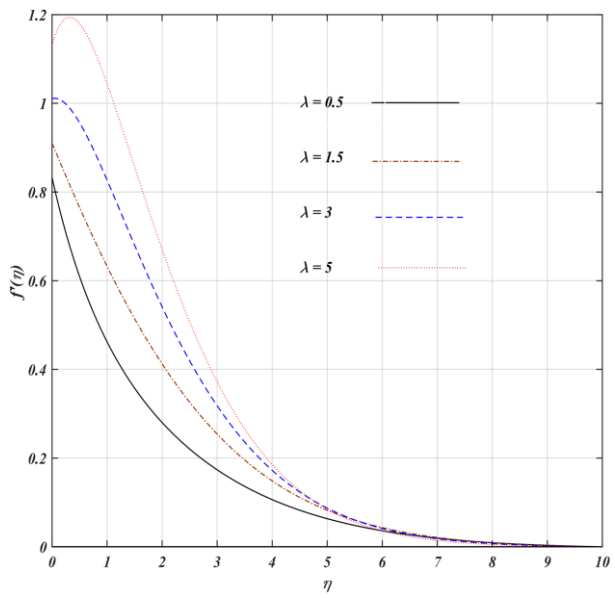

Fig. 10. Velocity profile change with λ.

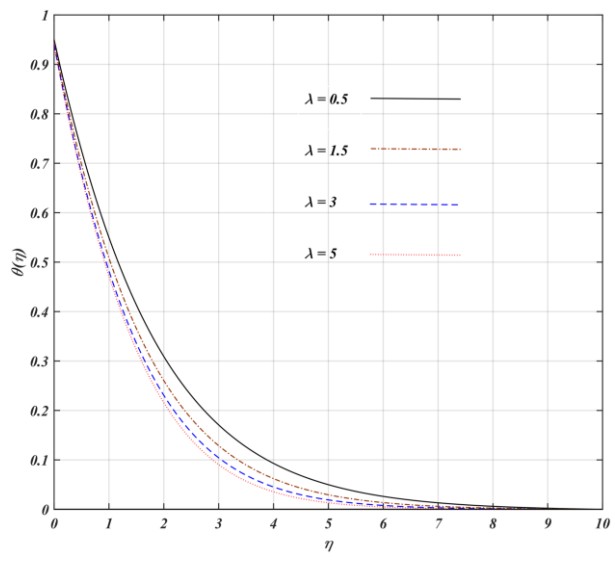

Fig. 11. Temperature profile change with λ.

Figure 12 shows the effect of the radiation parameter (N) on the temperature profile. An increase in N results in a continuous rise in temperature, because higher N enhances radiative heat transfer, increasing energy transport in the fluid. This leads to a higher temperature throughout the boundary layer. Figure 13 illustrates the effect of the Prandtl number (Pr) on temperature, showing a decrease in temperature as Pr increases. A higher Pr signifies greater thermal conductivity (κ), which lowers the fluid temperature.

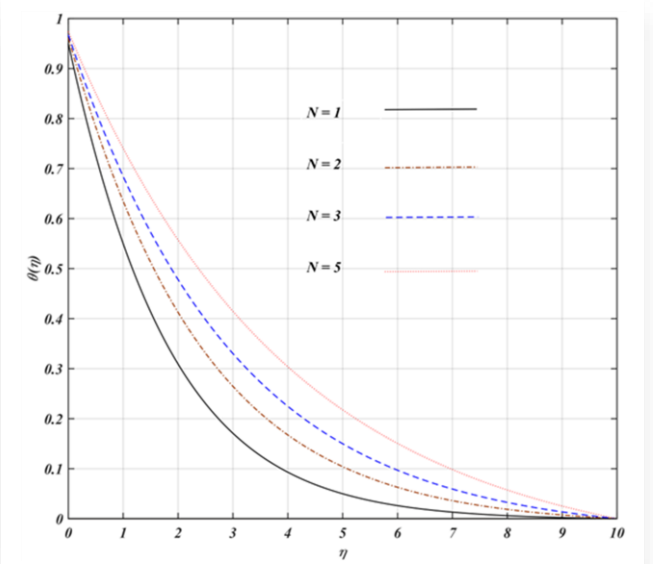

Fig. 12. Temperature profile change with N.

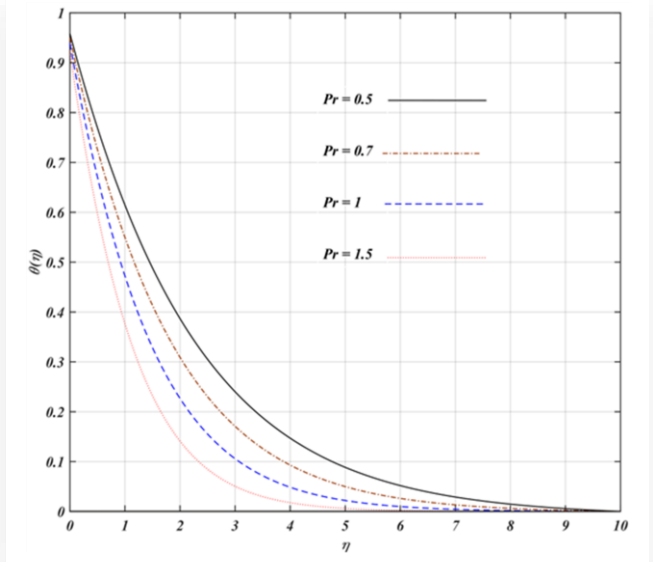

Fig. 13. Temperature profile change with Pr.

Figure 14 demonstrates that the temperature profile expands with an increase in the Eckert number (Ec). This is because Ec reflects the conversion of mechanical energy into thermal energy. When Ec is high, more mechanical energy is converted into heat, leading to a rise in the fluid temperature. Figure 15 examines the impact of the slip parameter for the temperature (λ_t), showing that temperature decreases with higher λ_t as less heat is transferred from the sheet to the fluid. The thermal boundary layer becomes thinner as less heat is conducted to the fluid. Figures 16 and 17 depict the influence of the velocity slip

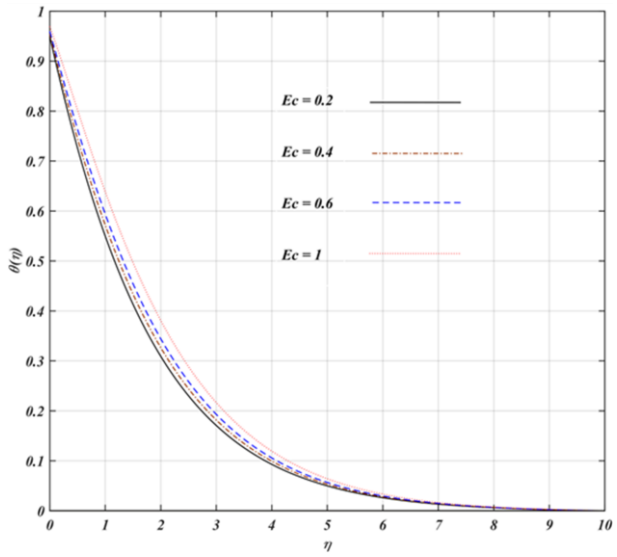

Fig. 14. Temperature profile change with Ec.

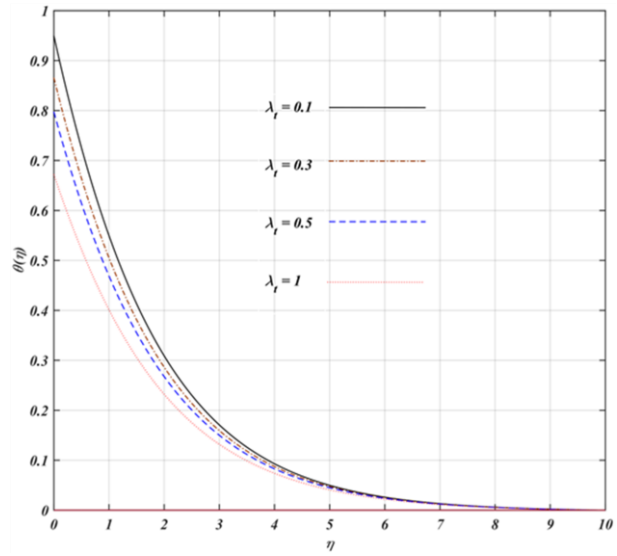

Fig. 15. Temperature profile change with λ_t.

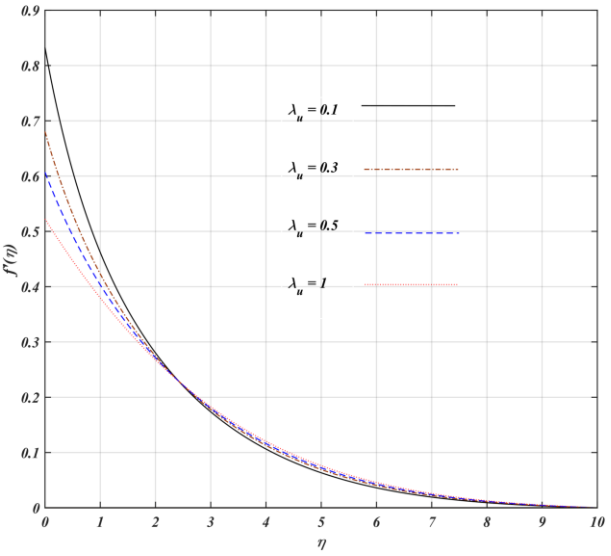

Fig. 16. Velocity profile change with λ_u.

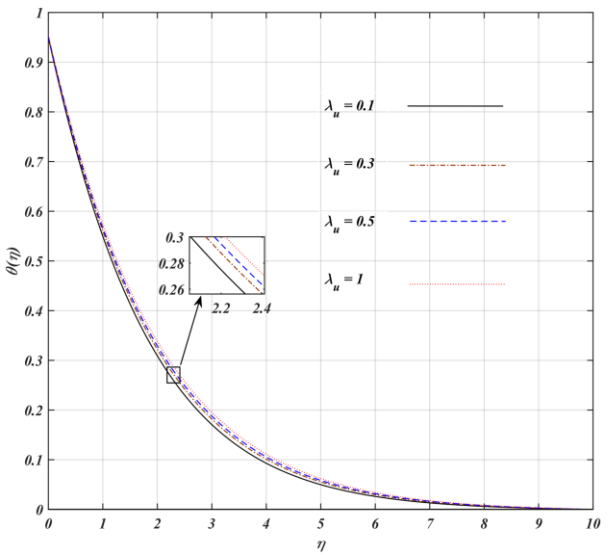

Fig. 17. Temperature profile change with λ_u.

parameter (λ_u) on the velocity and temperature. Velocity decreases with an increase in λ_u, because of a reduction in wall shear stress, but as η exceeds 2.4, it slightly increases due to the stretching effect of the sheet. Conversely, temperature is directly proportional to λ_u, increasing with λ_u. This results in an increase in thermal boundary layer thickness because of weaker momentum transfer.

The skin friction coefficient (C_f) and Nusselt (Nu) number play crucial roles in analysing the effects of shear stress and heat transfer at the surface of the stretching sheet. Table 2 summarizes the effect of various parameters on C_f and Nu for a fixed Reynolds number, Re = 1. The Nusselt number increases with S, Pr, β, and λ, but decreases with K_1, Fr, N, Ec, λ_u and λ_t. Meanwhile, the skin friction coefficient C_f increases with N, Ec, λ and λ_u, while it decreases with K_1, β, S, Fr, Pr and λ_t. A higher skin friction coefficient means increased drag force on the stretching sheet due to resistance from fluid motion. A higher Nusselt number implies more efficient heat transfer, which is crucial in applications like cooling processes and thermal management in industrial systems.

5. Practical significance and usefulness

The findings of this study offer valuable insights into the behaviour of Casson non-Newtonian fluid flow and heat transfer over a stretching sheet, considering various physical effects, such as porous media, thermal radiation, mixed convection, velocity slip and suction/blowing. These results have significant applications across multiple industrial and engineering fields, particularly in areas where non-Newtonian fluids and porous media play a crucial role.

The study demonstrates that parameters, such as the Prandtl number, suction parameter, Casson parameter and mixed convection parameter, notably enhance the Nusselt number, thereby improving heat dissipation. This is particularly important for cooling electronic devices, thermal coating processes and poly-

Table 2. $f''(0)$ and $-\theta'(0)$ for physical parameters β, λ, N, Pr, S, K_1, Fr, Ec, λ_u and λ_t.

K_1	β	S	Fr	N	Pr	Ec	λ	λ_u	λ_t	$f''(0)$	$-\theta'(0)$
0.1	0.5	0.5	1	1	0.7	0.2	0.5	0.1	0.1	-0.558356	0.499664
0.3	0.5	0.5	1	1	0.7	0.2	0.5	0.1	0.1	-0.626966	0.464039
0.5	0.5	0.5	1	1	0.7	0.2	0.5	0.1	0.1	-0.687742	0.433837
0.1	0.2	0.5	1	1	0.7	0.2	0.5	0.1	0.1	-0.383669	0.485282
0.1	0.4	0.5	1	1	0.7	0.2	0.5	0.1	0.1	-0.513380	0.497690
0.1	0.6	0.5	1	1	0.7	0.2	0.5	0.1	0.1	-0.595488	0.500780
0.1	0.5	0.0	1	1	0.7	0.2	0.5	0.1	0.1	-0.511995	0.430546
0.1	0.5	0.5	1	1	0.7	0.2	0.5	0.1	0.1	-0.558356	0.499664
0.1	0.5	1.0	1	1	0.7	0.2	0.5	0.1	0.1	-0.610393	0.499664
0.1	0.5	0.5	1	1	0.7	0.2	0.5	0.1	0.1	-0.558356	0.499664
0.1	0.5	0.5	3	1	0.7	0.2	0.5	0.1	0.1	-0.679037	0.451246
0.1	0.5	0.5	5	1	0.7	0.2	0.5	0.1	0.1	-0.769847	0.416987
0.1	0.5	0.5	1	1	0.7	0.2	0.5	0.1	0.1	-0.558356	0.499664
0.1	0.5	0.5	1	2	0.7	0.2	0.5	0.1	0.1	-0.538443	0.388077
0.1	0.5	0.5	1	3	0.7	0.2	0.5	0.1	0.1	-0.526579	0.327710
0.1	0.5	0.5	1	1	0.5	0.2	0.5	0.1	0.1	-0.543258	0.413735
0.1	0.5	0.5	1	1	0.7	0.2	0.5	0.1	0.1	-0.558356	0.499664
0.1	0.5	0.5	1	1	1.0	0.2	0.5	0.1	0.1	-0.575659	0.611694
0.1	0.5	0.5	1	1	0.7	0.2	0.5	0.1	0.1	-0.558356	0.499664
0.1	0.5	0.5	1	1	0.7	0.4	0.5	0.1	0.1	-0.554952	0.451332
0.1	0.5	0.5	1	1	0.7	0.6	0.5	0.1	0.1	-0.549534	0.403111
0.1	0.5	0.5	1	1	0.7	0.2	0.5	0.1	0.1	-0.558356	0.499664
0.1	0.5	0.5	1	1	0.7	0.2	1.5	0.1	0.1	-0.299004	0.556375
0.1	0.5	0.5	1	1	0.7	0.2	3.0	0.1	0.1	-0.034755	0.592747
0.1	0.5	0.5	1	1	0.7	0.2	0.5	0.1	0.1	-0.558356	0.499664
0.1	0.5	0.5	1	1	0.7	0.2	0.5	0.3	0.1	-0.355079	0.488848
0.1	0.5	0.5	1	1	0.7	0.2	0.5	0.5	0.1	-0.262017	0.480791
0.1	0.5	0.5	1	1	0.7	0.2	0.5	0.1	0.1	-0.558356	0.499664
0.1	0.5	0.5	1	1	0.7	0.2	0.5	0.1	0.3	-0.570966	0.447053
0.1	0.5	0.5	1	1	0.7	0.2	0.5	0.1	0.5	-0.581328	0.404767

extrusion, where efficient heat removal is essential to prevent overheating.

Additionally, the study examines the influence of the porosity parameter and local inertia coefficient on the velocity and temperature. This knowledge is beneficial in oil extraction, geothermal energy systems, and chemical filtration, where understanding fluid flow resistance through porous media is essential for optimizing performance.

The Casson fluid models are widely used to describe blood flow in arteries. The effects of suction and porosity on the velocity and temperature can provide insights into blood perfusion in biological tissues and aid in the design of porous medical implants for improved heat dissipation.

Furthermore, stretching sheet problems are common in polymer manufacturing, fibre spinning, and metal extrusion. The influence of mixed convection and porous media effects is also crucial in applications, such as solar energy collection, geothermal heat exchangers, and thermal energy storage systems.

6. Conclusions

The mathematical approaches of steady boundary layer flow for a radiating Casson fluid on a permeable stretching sheet under the existence of both velocity and temperature slip conditions with a Darcy-Forchheimer porous medium and viscous dissipation were analysed. The findings of the current investigation are briefly summarised below.

1) The velocity increases with increasing Ec and λ, but falls with increasing K_1, S > 0, β and Fr;
2) The temperature increases with an increase of K_1, Fr, N and λ_u, but declines with increasing λ, β, Pr, $S > 0$ and λ_t;
3) Fr first decreases the velocity, then as $\eta > 4.75$ (approximately) increases it due to the mixed convection effect. Boundary layer thickness increases with increasing local inertia coefficient;
4) The velocity profile enhances with increased β before $\eta = 0.62$ for $S = 0.5$ ($\eta = 0.86$ for $S = -0.5$), but after that, it decreases because of the slip velocity effect;
5) The velocity profile increases when λ increases, but the temperature decreases;
6) The skin friction coefficient C_f enhances with increasing values of N, Ec, λ and λ_u, while it reduces with a rise in values of K_1, β, S, Fr, Pr and λ_t;
7) Nu enhances with increasing values of S, Pr, β and λ, but decreases with rising values of K_1, Fr, N, Ec, λ_u and λ_t.

While the current study provides significant insights, several aspects require further exploration, such as three-dimensional flow effects, unsteady flow conditions, and nanofluid and hybrid nanofluid flow, chemical reaction and magnetic field effects.

References

[1] Gupta, P., & Gupta, P. (1977). Heat and mass transfer on a stretching sheet with suction or blowing. *Journal of Chemical Engineering*, 55(6), 744–746. doi: 10.1002/cjce.5450550619

[2] Magyari, E., & Keller, B. (1999) Heat and mass transfer in the boundary layers on an exponentially stretching continuous sur-

face. *Journal of Physics D: Applied Physics*, 32(5), 577–585. doi: 10.1088/0022-3727/32/5/012

[3] Elbashbeshy, E. (2001). Heat transfer over an exponentially stretching continuous surface with suction. *Archives of Mechanics*, 53(6), 643–651.

[4] Pramanik, S. (2014). Casson fluid flow and heat transfer past an exponentially porous stretching surface in presence of thermal radiation. *Ain Shams Engineering Journal*, 5(1), 205–212. doi: 10.1016/j.asej.2013.05.003

[5] Jain, R., Mehta, R., Mehta, T. & Yadav, R.S. (2020). Numerical study of chemically reactive MHD hydrodynamic boundary layer fluid flow over an absorptive surface in the presence of slip and mixed convection. *Advances in Mathematics: Scientific Journal*, 9(9), 7057–7064. doi: 10.37418/amsj.9.9.55

[6] Partha, M.K, Murthy, P.V., & Rajasekhar, G.P. (2005). Effect of viscous dissipation on the mixed convection heat transfer from an exponentially stretching surface. *Heat and Mass Transfer*, 41, 360–366. doi: 10.1007/s00231-004-0552-2

[7] Khan, S.K. (2006). Boundary layer viscoelastic fluid flow over an exponentially stretching sheet. *International Journal of Applied Mechanics and Engineering*, 11(2), 321–335.

[8] Sajid, M., & Hayat, T. (2008). Influence of thermal radiation on the boundary layer flow due to an exponentially stretching sheet. *International Communications in Heat and Mass Transfer*, 35(3), 347–356. doi: 10.1016/j.icheatmasstransfer.2007.08.006

[9] Bejawada, S.G., Reddy, Y.D., Jamshed, W., Nisar, K.S., Alharbi, A.N., & Chouikh, R. (2022). Radiation effect on MHD Casson fluid flow over an inclined non-linear surface with chemical reaction in a Forchheimer porous medium. *Alexandria Engineering Journal*, 61(10), 8207–8220. doi: 10.1016/j.aej.2022.01.043

[10] Rasool, G., Chamkha, A.J., Muhammad, T., Shafiq, A., & Khan, I. (2020). Darcy-Forchheimer relation in Casson type MHD nanofluid flow over non-linear stretching surface. *Propulsion and Power Research*, 9(2), 159–168. doi: 10.1016/j.jppr.2020.04.003

[11] Bilal Ashraf, M., Hayat, T. & Alsaedi, A. (2017). Mixed convection flow of Casson fluid over a stretching sheet with convective boundary conditions and Hall effect. *Boundary Value Problems*, 137. doi: 10.1186/s13661-017-0869-7

[12] Raju, C.S., Hoque, M.M., & Sivasankar, T. (2017). Radiative flow of Casson fluid over a moving wedge filled with gyrostatic microorganisms. *Advanced Powder Technology*, 28(2), 575–583. doi: 10.1016/j.apt.2016.10.026

[13] Mehmood, R., Rana, S., Akbar, N.S., & Nadeem, S. (2018). Non-aligned stagnation point flow of radiating Casson fluid over a stretching surface. *Alexandria Engineering Journal*, 57(2), 939–946. doi: 10.1016/j.aej.2017.01.010

[14] Sinha, S., & Yadav, R.S. (2022). MHD mixed convective slip flow along an inclined porous plate in presence of viscous dissipation and thermal radiation. *Trends in Sciences*, 19(4), 2685. doi: 10.48048/tis.2022.2685

[15] Loganathan, P., & Deepa, K. (2019). Electromagnetic and radiative Casson fluid flow over a permeable vertical Riga-plate. *Journal of Theoretical and Applied Mechanics*, 57(4), 987– 998. doi: 10.15632/jtam-pl/112421

[16] Kumar, K.A., Sugunamma, V., & Sandeep, N. (2020). Effect of thermal radiation on MHD Casson fluid flow over an exponentially stretching curved sheet. *Journal of Thermal Analysis and Calorimetry*, 140, 2377–2385. doi: 10.1007/s10973-019-08977-0

[17] Samrat, S.P., Reddy, M.G., & Sandeep, N. (2021). Buoyancy effect on magnetohydrodynamic radiative flow of Casson fluid with Brownian moment and thermophoresis. *The European Physical Journal Special Topics*, 230, 1273–1281. doi: 10.1140/epjs/s11734-021-00043-x

[18] Gebhart, B. (1962). Effects of viscous dissipation in natural convection. *Journal of fluid Mechanics*, 14(2), 225–232. doi: 10.1017/S0022112062001196

[19] Al-Hadhrami, A., Elliott, L. & Ingham, D. (2003). A new model for viscous dissipation in porous media across a range of permeability values. *Transport in Porous Media*, 53, 117–122. doi: 10.1023/A:1023557332542

[20] Hayat, T., Khan, M.I., Waqas, M., Yasmeen, T., & Alsaedi, A. (2016). Viscous dissipation effect in flow of magnetonanofluid with variable properties. *Journal of Molecular Liquids*, 222, 47–54. doi: 10.1016/j.molliq.2016.06.096

[21] Kumar, P., Yadav, R.S, & Makinde, O.D. (2023). Numerical study of Williamson fluid flow and heat transfer over a permeable stretching cylinder with the effects of joule heating and heat generation/absorption. *Heat Transfer*, 52(4), 3372–3388. doi: 10.1002/htj.22832

[22] Koo, J., & Kleinstreuer, C. (2004). Viscous dissipation effects in microtubes and microchannels. *International Journal of Heat and Mass Transfer*, 47(14-16), 3159–3169. doi: 10.1016/j.ijheatmasstransfer.2004.02.017

[23] Winter, H.H. (1987). Viscous dissipation term in energy equations. American Institute of Chemical Engineers, *Modular Instruction, Series C: Transport, Vol. 7. Calculation and Measurement Techniques for Momentum, Energy and Mass Transfer*, 27–34.

[24] Khan, M.I., Alzahrani, F., & Hobiny, A. (2020). Simulation and modeling of second order velocity slip flow of micropolar ferrofluid with Darcy-Forchheimer porous medium. *Journal of Materials Research and Technology*, 9(4), 7335–7340. doi: 10.1016/j.jmrt.2020.04.079

[25] Mukhopadhyay, S., De, P.R., Bhattacharyya, K & Layek, G.C. (2012). Forced convective flow and heat transfer over a porous plate in a Darcy-Forchheimer porous medium in presence of radiation. *Meccanica*, 47, 153–161. doi: 10.1007/s11012-011-9423-3

[26] Kumar, K.G., Reddy, M.G., Khan, M.I., Alzahrani, F., Khan, M.I., & El-Zahar, E.R. (2021). Heat transfer and melting flow of a Reiner-Philippoff fluid over a surface with Darcy-Forchheimer medium. *Case Studies in Thermal Engineering*, 28, 101649. doi: 10.1016/j.csite.2021.101649

[27] Prasad, D.K., Chaitanya, G.K., & Raju, R.S. (2019). Double diffusive effects on mixed convection Casson fluid flow past a wavy inclined plate in presence of Darcian porous medium. *Results in Engineering*, 3, 100019. doi: 10.1016/j.rineng.2019.100019

[28] Shoaib, M., Kausar, M., Nisar, K.S., Raja, M.A.Z., & Morsy, A. (2022). Impact of thermal energy on MHD Casson fluid through a Forchheimer porous medium with inclined non-linear surface: A soft computing approach. *Alexandria Engineering Journal*, 61(12), 12211–12228, doi: 10.1016/j.aej.2022.06.014

[29] Bansal, S., & Yadav, R.S. (2024). Effect of slip velocity on Newtonian fluid flow induced by a stretching surface within a porous medium. *Journal of Engineering and Applied Science*, 71, 153. doi: 10.1186/s44147-024-00481-z

[30] Sahoo. B., & Poncet, S. (2011). Flow and heat transfer of a third grade fluid past an exponentially stretching sheet with partial slip boundary condition. *International Journal of Heat and Mass Transfer*, 54(23-24), 5010–5019. doi: 10.1016/j.ijheatmasstransfer.2011.07.015

[31] Bidin, B., & Nazar, R. (2009). Numerical solution of the boundary layer flow over an exponentially stretching sheet with thermal radiation. *European Journal of Scientific Research*, 33(4), 710–717.